

Waveguide-coupled AlGaAs/GaAs microcavity ring and disk resonators with high finesse and 21.6-nm free spectral range

D. Rafizadeh, J. P. Zhang, S. C. Hagness, A. Taflove, K. A. Stair, and S. T. Ho

Department of Electrical and Computer Engineering, McCormick School of Engineering, Northwestern University,
2145 Sheridan Road, Evanston, Illinois 60208

R. C. Tiberio

Cornell Nanofabrication Facility, Cornell University, Ithaca, New York 14853-5403

Received March 31, 1997

We report the realization and demonstration of novel semiconductor waveguide-coupled microcavity ring and disk resonators. For a 10.5- μm -diameter disk resonator, we measure a finesse of 120, a resonant linewidth of 0.18 nm, and a free-spectral range of 21.6 nm in the 1.55- μm -wavelength region. We present the nanofabrication methods and the experimental results for 10.5- and 20.5- μm -diameter ring and disk resonators to show the feasibility of such devices. © 1997 Optical Society of America

Nanofabrication makes it possible to realize optical microcavity ring or disk resonators that can serve as micrometer-sized switches or multiplexers–demultiplexers, as was proposed recently.^{1,2} One can integrate these resonators with other micrometer-sized components such as the recently described photonic-wire laser³ to form photonic integrated circuits. Microcavity resonators may also be useful in applications in which a wide free-spectral range, $\Delta\lambda_{\text{fsr}}$, is desired, such as a filter that is tunable over the 30-nm erbium bandwidth. Previous ring resonators based on weakly guiding waveguides are restricted to diameters of >3 mm because of high radiative bending losses, resulting in a $\Delta\lambda_{\text{fsr}}$ of <0.8 nm.^{4,5} However, a 5- μm -diameter resonator based on strongly guiding waveguides can have a $\Delta\lambda_{\text{fsr}}$ of approximately 45 nm. With strong lateral confinement, the disk or the ring microcavity resonator can have a very small (1–2 μm) diameter with negligible bending loss.⁶

A typical geometry of a microcavity resonator is shown in Fig. 1(a). Light traveling in a waveguide (WG1) is coupled into an adjacent ring or disk through a small gap c by resonant waveguide coupling. The light propagates around the resonator and is coupled out through WG2. On-resonance light is switched from port X to port Y (transmission), and off-resonance light exits from port Z (reflection). The potential advantage of this ring geometry over a Fabry–Perot-type resonator is that there is no feedback of the off-resonance light from the resonator.

The waveguide structure is grown upon a GaAs substrate by molecular-beam epitaxy, starting with a 2- μm -thick buffer layer of $\text{Al}_x\text{Ga}_{1-x}\text{As}$ ($x = 0.4$), followed by a 0.45- μm GaAs guiding layer and a 0.25- μm top cladding layer of $\text{Al}_x\text{Ga}_{1-x}\text{As}$ ($x = 0.4$).

The key microcavity resonator design parameters are the coupling efficiency and the waveguide-propagation loss (which is mainly due to sidewall roughness). Strong waveguiding confinement dictates that the resonator-to-waveguide gap has to be very small for adequate evanescent coupling. Based

on current nanofabrication technology, a realistic gap width should be ≥ 0.1 μm . For good transmission characteristics, the total resonator coupling should be greater than the round-trip cavity loss. The desired range of coupling is typically 0.5–3%, depending on the waveguide propagation loss. The coupling efficiency is a function of the coupling length, the waveguide structure, and the gap width.⁷ For a waveguide width of 0.5 μm , a thickness of 0.45 μm , and a gap width of 0.1 μm , the calculated coupling is 2.5% for an effective coupling length of 1 μm .

From the measured transmission Fabry–Perot resonances from the end facets of separate waveguides, the TM waveguide intensity propagation loss α is 3.2/cm for a 0.5- μm -wide waveguide. From this value, we estimate a 1.2% round-trip loss in the 10.5- μm -diameter ring resonator. The disk resonator has the advantage of lower scattering loss (potentially half that of the ring) since only the outer-rim sidewall is etched.

For the microdisk resonator, the mode size supported by the adjacent waveguide must match the whispering-gallery-mode (WGM) width propagating in the disk. Proper mode matching will support single-mode behavior within the disk and optimize disk-to-waveguide

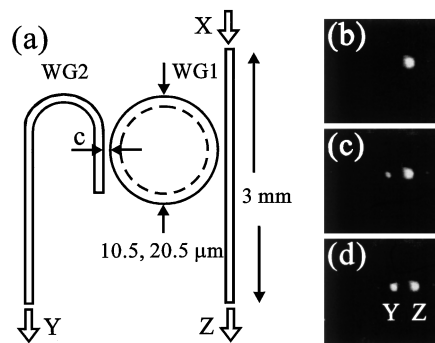


Fig. 1. (a) Illustration of the fabricated ring or disk resonator geometry and (b)–(d) infrared camera images showing switching of light from port Z to port Y at the 1555.6-nm resonance of the 10.5- μm -diameter disk.

coupling. Here we use conformal transformation to calculate the lowest-order WGM width.⁸ For 10.5- and 20.5- μm disks, the calculated adjacent waveguide widths to match the WGM widths are 0.5 and 0.6 μm , respectively.

The scanning electron microscope (SEM) images in Fig. 2 are 10.5- μm -diameter disk and ring resonators. The adjacent waveguides are 2 μm wide at each end and gradually taper to 0.5 μm near the ring or disk. The fabricated gap widths are 0.1 μm . As can be seen in the SEM images, we created the resonators and waveguides by etching a 1- μm -wide trench that defines and isolates the patterns.

The patterns were created upon a poly(methyl methacrylate) resist layer by electron-beam lithography (JEOL JBX 5DII), and the AlGaAs/GaAs was etched with chemically assisted ion-beam etching (CAIBE). The electron-beam lithography exposure conditions were a 300-pA probe current, a 50-eV acceleration potential, an 80 $\mu\text{m} \times 80 \mu\text{m}$ field, and an 11-mm working distance. The poly(methyl methacrylate) mask was transferred to an underlying SiO₂ layer by use of reactive ion etching to provide a durable mask capable of withstanding the CAIBE process. The CAIBE parameters were a beam voltage of 500 V, a beam current density of 0.14 mA/cm², a chlorine flow rate of 15 SCCM (SCCM denotes cubic centimeters per minute at STP), an argon flow rate of 2 SCCM, and an elevated substrate temperature of 100 °C. Following the CAIBE etch, the remaining SiO₂ mask was removed from the sample. The resonators were etched to a depth of 2.2 μm at an etch rate of 0.1 $\mu\text{m}/\text{min}$. Mask erosion was minimal; gaps patterned to be 0.07 μm were measured to be 0.1 μm under the SEM. The sidewall roughness (vertical striations) observed under the SEM is 10–20 nm.

The waveguide setup uses an end-fire method to couple light from a tunable laser diode into the cleaved waveguide end facets. Two lenses with a numerical aperture of 0.55 and a focal length of 4.5 mm focus the input light to the waveguide input end (port X) and collimate the waveguide output light. As illustrated in Fig. 1(a), port Y is curved 180° so that both ports Y and Z are in the output direction. Figure 1(b) shows the waveguided output spot from port Z (resonator reflection) imaged with an infrared vidicon camera. In Fig. 1(c), as the laser diode is tuned to on-resonance at 1555.6 nm, the resonant light begins to appear at port Y. In Fig. 1(d), the on-resonance light at port Y (transmission) is 40–50% of the input light.

Strong resonances were observed for the TM mode but not for the TE mode. For the TE mode, the 1- μm -wide trench that defines the patterns (as can be seen in the SEM images) was not sufficient to isolate the waveguide structures. We found high lateral coupling of TE light to the surrounding media, translating into greater α for the TE mode.

For detection and measurement of the resonances, the waveguide output was apertured and detected with a large-area germanium detector and a lock-in amplifier. The spectral scan rate and the sampling rate give a resolution of 0.02 nm. Figure 3 shows the measured reflectivity (port Z) from the 10.5- μm

disk; the resonant wavelengths are 1534.4, 1555.6, and 1577.2 nm. We normalized the data to remove the 3-mm-long waveguide Fabry–Perot resonances and the 10–20% 1-nm modulation from the laser diode source. The measured $\Delta\lambda_{\text{fsr}}$ is 21.6 nm for the 10.5- μm disk.

The calculated reflectivity is

$$1 - \frac{t_{\text{max}}}{1 + F \sin^2[2\pi n_{\text{eff}}(\lambda)l/\lambda_0]},$$

where $F = 4RA/(1 - RA)^2$, $t_{\text{max}} = (1 - R)^2A/(1 - RA)^2$, $A = \exp(-\alpha l)$, l is $\pi D_{\text{eff}}/2$, R is (1 - coupling), and n_{eff} is the effective index of refraction. D_{eff} is the effective disk or ring diameter corresponding to the circumferential path traveled by the peak of the guided mode. The free spectral range is

$$\Delta\lambda_{\text{fsr}} = \frac{n_{\text{eff}}(\lambda_m)2l}{m} - \frac{n_{\text{eff}}(\lambda_{m+1})2l}{m+1}.$$

For the 10.5- μm disk case, we calculate $\Delta\lambda_{\text{fsr}} = 21.4$ nm with $n_{\text{eff}}(1577.2 \text{ nm}) = 3.1532$; $n_{\text{eff}}(1555.6 \text{ nm}) = 3.1597$ for m , $m + 1 = 63, 64$; and an estimated $D_{\text{eff}} = 10 \mu\text{m}$.

Figure 3 also shows the calculated reflectivity for the 10.5- μm disk. Using the estimated $\alpha = 1.6/\text{cm}$ (half of the α measured for the ring) and $R = 0.98$ to match the finesse, we find that the maximum transmission t_{max} is higher than the experimental

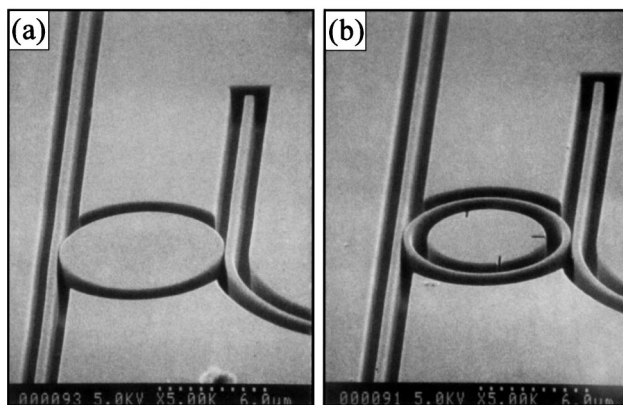


Fig. 2. SEM images of a 10.5- μm -diameter (a) disk and (b) ring.

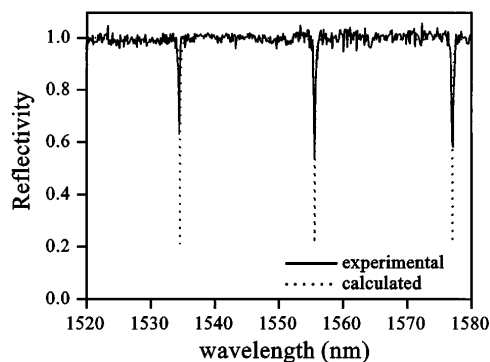


Fig. 3. Measured (experimental) and calculated reflectivity, showing resonances from a 10.5- μm disk with 2% coupling and $\alpha = 1.6/\text{cm}$.

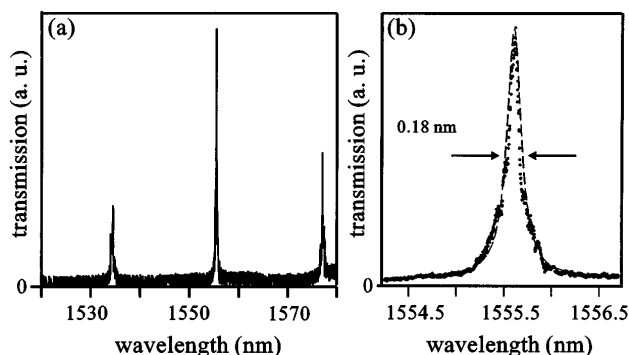


Fig. 4. (a) Measured transmission of the 10.5- μm -diameter disk. (b) Fine-resolution spectral scan of the 10.5- μm -disk transmitted peak centered at 1555.6 nm and the calculated transmission (dotted curve).

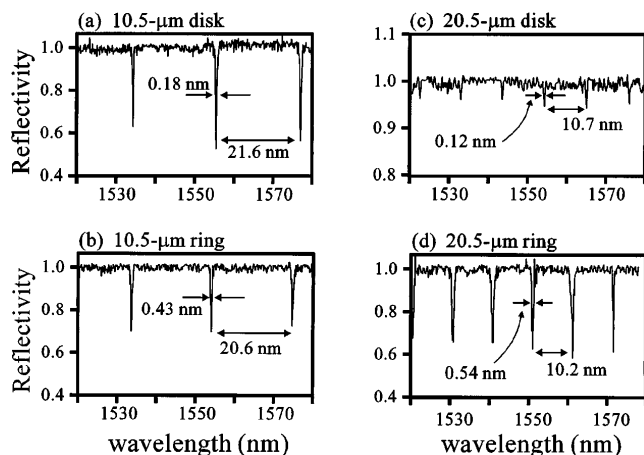


Fig. 5. Reflectivity of the (a) 10- μm disk, (b) 10.5- μm ring, (c) 20.5- μm disk, and (d) 20.5- μm ring. $\Delta\lambda_{\text{FWHM}}$ (\rightarrow) and $\Delta\lambda_{\text{fsr}}$ (\leftrightarrow) are indicated in the graphs.

value. The lower experimental t_{max} may be the result of one or all of the following factors: First, asymmetric coupling on either side of the disk or ring (owing to fabrication irregularities) can lead to unbalanced mirrors and a reduced t_{max} . Second, greater loss than predicted (closer to $\alpha = 6/\text{cm}$ in the disk and $\alpha = 15/\text{cm}$ in the ring to match the experimental t_{max}) could be the result of higher coupling loss across the 1- μm trench (since the mode in the curved rings and disks travels closer to the outer edge) or higher scattering loss from the disk or ring outer edge.

Figure 4(a) shows the (nonnormalized) transmission measurement from port Y for the same 10.5- μm disk. The fine-resolution scan in Fig. 4(b) across the transmitted peak centered at 1555.6 nm shows the FWHM ($\Delta\lambda_{\text{FWHM}}$) to be 0.18 nm wide (with 0.003-nm resolu-

tion). Figure 5 shows the reflectivity for each resonator. All the gap widths are 0.1 μm . The finesse values for the 10.5- μm disk and ring are 120 and 48, respectively, and the finesse values for the 20.5- μm disk and ring are 89 and 18, respectively. In the ring cases the linewidths are wider owing to the higher scattering loss from the added inner sidewall. In the 20.5- μm -disk case the maximum transmission is very low because the adjacent 0.8- μm -wide waveguide is too wide for proper matching to the WGM width in the disk, resulting in low coupling.

In conclusion, we have used nanolithography methods to fabricate and demonstrate waveguide-coupled 10.5- and 20.5- μm -diameter AlGaAs/GaAs ring and disk microcavity resonators. The 10.5- μm -diameter disk resonator has a wide 21.6-nm free-spectral range, a finesse of 120, and a cavity Q greater than 8500. We believe that these results are an important step toward developing photonic integrated circuits. Nanoscale optical resonators with a ring or a disk geometry can be as small as 1 to 2 μm in diameter without substantial radiation loss (and may potentially yield high finesse and free-spectral ranges approaching 100 nm). The microdisk resonator is especially promising because of potentially low scattering loss. The devices have the potential to be electro-optically tunable by induced refractive-index changes of the cavity.

This research was supported by the U.S. Air Force Office of Scientific Research/Advanced Research Projects Agency under contract F49620-96-1-0262 and National Science Foundation Faculty Early Career Development Award ECS-95024975.

References

1. D. Rafizadeh, J. P. Zhang, L. Wang, S. C. Hagness, A. Taflove, R. C. Tiberio, and S. T. Ho, paper ThP4 presented at the Optical Society of America Annual Meeting, Rochester, New York, October 20–25, 1996.
2. S. C. Hagness, D. Rafizadeh, S. T. Ho, and A. Taflove, paper ThZ4 presented at the Optical Society of America Annual Meeting, Rochester, New York, October 20–25, 1996.
3. J. P. Zhang, D. Y. Chu, S. L. Wu, W. G. Bi, R. C. Tiberio, C. W. Tu, and S. T. Ho, *IEEE Photon. Technol. Lett.* **8**, 968 (1996).
4. T. Kominato, Y. Hibino, and K. Onose, *IEEE Photon. Technol. Lett.* **5**, 560 (1993).
5. K. Oda, S. Suzuki, H. Takahashi, and H. Toba, *IEEE Photon. Technol. Lett.* **6**, 1031 (1994).
6. E. A. J. Marcatili, *Bell Syst. Tech. J.* **48**, 2103 (1969).
7. E. A. J. Marcatili, *Bell Syst. Tech. J.* **48**, 2071 (1969).
8. M. K. Chin, D. Y. Chu, and S. T. Ho, *J. Appl. Phys.* **75**, 3302 (1994).